Quantitative Analysis of Breast Cancer NACT Response on DCE-MRI Using Gabor Filter Derived Radiomic Features

https://doi.org/10.3991/ijoe.v18i12.32501

Priscilla Dinkar Moyya, Mythili Asaithambi(✉)
School of Electronics Engineering, Vellore Institute of Technology, Vellore, Tamil Nadu, India
mythili.asaithambi@vit.ac.in

Abstract—In this work, an attempt has been made to quantify the treatment response due to Neoadjuvant Chemotherapy (NACT) on the publicly available QIN-Breast of TCIA database (N = 25) using Gabor filter derived radiomic features. The Gabor filter bank is constructed using 5 scales and 7 orientations. Different radiomic features were extracted from Gabor filtered Dynamic Contrast Enhanced Magnetic Resonance images (DCE-MRI) of patients having 3 different visits (Visit 1: before, Visit 2: after 1st cycle, and Visit 3: the last cycle of NACT). The extracted radiomic features were analyzed statistically and Area Under Receiver Operating Characteristic (AUROC) has been calculated. Results show that the Gabor derived radiomic features could differentiate the pathological differences among all three visits. Energy has shown a significant difference between all the three orientations particularly between Visits 2 & 3. However, Entropy from $\lambda = 2$ and $\theta = 30°$ between Visit 2 & 3, Skewness from $\lambda = 2$ and $\theta = 120°$ between Visit 1 & 3 could differentiate the treatment response with high statistical significance of $p = 0.006$ and 0.001 respectively. From the ROC analysis, the better predictors were Short Run Emphasis (SRE), Short Zone Emphasis (SZE), and Energy between Visit 1 & 3 by achieving an AUROC of 76.38%, 75.16%, and 71.10% respectively. Further, the results suggest that the radiomic features are capable of quantitatively comparing the breast NACT prognosis that varies across multi-oriented Gabor filters.

Keywords—breast cancer, DCE-MRI, Gabor filter bank, Neoadjuvant Chemotherapy, radiomic features, treatment response

1 Introduction

Breast cancer is a widespread malignant disease found in women worldwide [1]. Breast cancer patients may have a better chance of surviving if they are properly screened and diagnosed early during NACT treatment. In treating locally advanced breast cancers, NACT is frequently used as a protective barrier administered before the surgery, which can reduce the tumor size and metastasis and enhance surgical choices. The optimum response of NACT is perhaps the absence of residual cancer

burden within the invasive breast tumor cells also known as Pathological Complete Response (PCR), which substantially predicts a better prognosis than patients who have an inadequate response (non-PCR) [2].

Various imaging methods have been utilized to assess the pathological response in patients with breast cancer to NACT, including ultrasonography, mammography, breast magnetic resonance imaging (MRI), and positron emission tomography/computed tomography (PET/CT) [3]. MRI is particularly useful for identifying the severity in the breast, and it is frequently used in the NACT to assess the treatment, predict, and prognose the tumor response. This modality was found to be more accurate than conventional imaging techniques in predicting the presence of cancer burden after NACT treatment [4]. This technique has high sensitivity besides its specificity, due to the reason that it fails to screen the dense breast tissues. A T1 weighted acquisition protocol, DCE-MRI with Contrast Agent administration, is frequently used to image dense breasts. DCE-MRI can image the full breast volume in comparison to conventional methods along with kinetic curve analysis which makes it an ideal supplementary imaging tool for breast treatment. When DCE-MRI is combined with NACT, it can be used to enhance the functional tumor properties in addition to the structural properties of the tumor that acts as a potential indicator for the treatment response. However, the approaches to compute DCE-MRI metrics, whether semi quantitative or quantitative, cannot capture the spatial heterogeneity of the tumor functions, and therefore, valuable information could be missed during therapeutic response evaluation [5–7].

More acceptable quantitative approaches for assessing the tumor response to NACT treatment were developed as a result of insufficient size-based quantifying methods [8]. Texture-based image features have been widely used in recent years for quantifying tumor heterogeneity and predicting the therapy response of breast cancer patients [9–11]. Radiomics, which can extract the quantitative features from the medical images that characterize the spatial relationship in the tumor regions, is used among various types of cancers and scanning techniques. The integration of radiomic features with the significant tumor properties, clinical, and genomic data could be identified, allowing for more accuracy in clinical practice [12]. There are four main texture analysis techniques (i) statistical (ii) structural (iii) model-based and (iv) transform-based. The spatial distribution of image pixels can be calculated by statistical method, the structural method depends on the geometrical attributes of the image, model-based utilizes stochastic models, and transform-based analysis depends on temporal filtering techniques [13]. This research focuses on transformed-based techniques, particularly a Gabor filtering technique that can quantitatively evaluate the texture at various scales and orientations. In addition, radiomic features are extracted to analyze the performance of predicting breast cancer treatment response and to assess the classification accuracy of individual scale and orientation pairs.

Dennis Gabor first invented Gabor filters in 1946, and 42 years later J. Daugman developed a 2-Dimensional Gabor filter that achieves a coordinated optimal resolution in the spatial and frequency spaces [14]. Several computer vision experts contend that the scale and orientation of Gabor filters are analogous to human vision. In the last few decades, these filters have been used in image analysis, image compression, segmentation, edge detection, fingerprint, face recognition, and texture analysis.

The configuration of Gabor filter bank parameters is a typical problem in these applications [15–17]. A simple Gabor filter may detect texture patterns with a single scale and orientation, but to define complicated texture patterns, multiple orientations and scales must be created and acquired. Previous studies often use the same parameters because they consistently produce satisfactory results [18,19]. The Gabor filter for classifying the texture of satellite images yielded results up to 70% and when used the GLCM features along with the Gabor filter provided the best accuracy of classification with 80%. Likewise, Gabor filters can enhance absoluteness when multiple orientations and scales are considered. These aspects explain that the texture is depending on frequency and orientation that has to be properly handled in the evolving radiomic field.

A few breast cancer studies for the classification and prediction of NACT treatment response using Gabor filters have been implemented. Different feature sets such as texture features which include Haralick, Co-occurrence of Local Anisotropic Gradient Orientations (CoLlAGe) features, Law features and Gabor features from intra- and peri-tumoral regions of breast DCE-MRI data and evaluated the ability of extracted features to predict PCR to NACT. Among the ten prominent radiomic features with discriminating capability, three Gabor features are also reported in the intratumoral areas [20]. Similarly, the performance of radiomic analysis for pretreatment prediction of NACT response is carried out by extracting morphological, first order, Gabor, and Law features from multiparametric MRI data. Only Gabor and Law's features are selected for the final radiomic analysis of the treatment. That may be because these high-dimensional descriptors acquired more precise tumor textural information, making them better for the prediction of treatment response [21].

In this work, Gabor filter derived radiomic features are used to analyze the quantitative study of breast cancer NACT response on DCE-MR images. Radiomic features from each scale orientation are calculated and individual treatment visits are compared concerning NACT treatment response. Further, the ROC analysis is carried out to assess the predictive performance ability of the significant radiomic features.

2 Materials and methods

2.1 Patient and protocol information

The data used in this work is obtained from the Quantitative Imaging Network (QIN) Breast of The Cancer Imaging Archive (TCIA) [22], which is maintained by a US university center. The dataset contains DCE-MRI, DWI-MRI, and PET/CT from 68 patients, in which DCE-MRI data of 25 patients with three visit data are considered for this study. The analysis is based on baseline evaluations of 11 PCR and 14 non-pCR subjects. Images were acquired at three time points (i) prior to the start of the treatment (Visit 1), (ii) after the first cycle of treatment (Visit 2), and (iii) after completion of all treatments (prior to surgery) (Visit 3). Table 1 summarizes the dataset breakdown by pathological response status of the study population.

Table 1. Dataset breakdown by pathological response status

	PCR	**non-PCR**
No. of Subjects	11	14
Age	43 ± 6.37 (mean ± SD)	48.57 ± 9.43 (mean ± SD)
Weight	48.57 ± 9.43	72.4 ± 16.53
Estrogen Receptor		
Positive	1	7
Negative	9	7
Progesterone		
Positive	1	7
Negative	9	7
HER2		
Positive	4	5
Negative	6	9
Tumor Grade		
I	–	2
II	2	4
III	9	8

Note: SD-Standard Deviation.

The MRI data examination was performed on Philips 3T Achieva MR scanner (Philips Healthcare, Best, The Netherlands) using 16 channel bilateral breast coil. The acquisition parameters of this data include flip angle of 20°, Repetition time (TR) of 7.9 ms, Echo time (TE) of 4.6 ms, acquisition matrix of 192×192×20, sagittal Field of view (FOV) of 22×22 cm^2, and slice thickness of 5 mm as reported elsewhere [23]. For this study, 25 dynamic scans are acquired at the temporal resolution of 16 sec. After the baseline scans, the contrast agent gadopentetate dimeglumine (Gd-DTPA) was placed within an antecubital vein delivered at 0.1 mmol/kg (9–15 mL, depending on patient weight) at 2 mL/sec via a power injector.

2.2 Gabor filter design

A basic Gabor filter is defined as a product of a complex sinusoidal wave multiplied by a Gaussian kernel [24]. A two-dimensional Gabor filter is given as,

$$g = e^{\frac{-1}{2}\left(\frac{x'^2}{\sigma_x^2}+\frac{y'^2}{\sigma_y^2}\right)} e^{(i(2\pi\lambda'+\varphi))} \tag{1}$$

Where $x' = (x\cos\theta + y\sin\theta)$; $y' = (-x\sin\theta + y\cos\theta)$

λ-spatial frequency (scale), θ-Orientation of the Gabor filter, φ-phase offset of the harmonic factor and σ_x, σ_y are standard deviations along x and y directions.

In this analysis, for designing the Gabor filter bank five scales and seven orientations are selected. The scale is chosen as a multiple of 2 and the orientation is within the range of (0,2π) degrees [24]. Hence five scales λ = (2,4,8,16,32) and

$\theta = (0°,30°,60°,90°,120°,135°,150°)$ are considered for this study. However, the tumor areas of different subjects vary with respect to the severity of the breast cancer, thus a smaller scale value is required to extract more detailed textures from the images. Similarly, the orientations are selected from 0 to π degrees, as π-2π degrees replicate the same information as from 0-π. So, $\lambda = 2$ and $\theta = 0°$, 30°, 60°, 90°, 120°, 135°, and 150° are considered for this study resulting in seven filters in a Gabor filter bank. The design of scale and orientation frequently vary depending on the applications. A recent study has demonstrated that Gabor features of two different combinations of scale and orientation are shown to predominant discrimination in predicting the response in intra-tumoral regions [20]. Since the two combinations $\lambda = 2$, $\theta = 30°$, and $\lambda = 2$, $\theta = 135°$ are used for prediction, this can be useful to observe the individual treatment responses of Visit 1, Visit 2, and Visit 3 of NAC treatment.

The stated Gabor filter bank is used on the DCE-MRI exams of 25 breast cancer patients over three visits. The time-point selection of the DCE procedure is much more important, which will expect rich texture information after the peak enhancement. This hypothesis is tested by calculating the mean intensity of the subjects at every 25 time points of the data by using MATLAB software. The maximum mean intensity time point is selected for applying a Gabor filter bank. The application of Gabor bank on DCE-MRI time point of maximum intensity results in three scale-orientation image sets. Different orientations indicate varying texture features, whereas, the scale parameter ($\lambda = 2$) will provide finer texture details.

2.3 Radiomic feature extraction

Radiomic features are extracted from each scale-oriented Gabor filtered image to assess the stability of every radiomic feature with respect to the associated features after the response of every treatment visit. All radiomic features are calculated for the 3-dimensional volume of Gabor filtered image of three different scale-orientations [25]. A total of 38 radiomic features from each Gabor filtered image include: (i) 3 global features which calculate the distribution of image intensities, (ii) 9 Gray Level Co-occurrence Matrix (GLCM) features that describe the image properties associated with second-order statistics, (iii) 13 Gray Level Run Length Matrix (GLRLM) related to the distribution of gray-levels of runs and (iv) 13 Gray Level Size Zone Matrix (GLSZM) that uses size zone of the observed area.

2.4 Statistical analysis

The student's t-test was used to all radiomic features at different scale and orientation filtered images to uncover the potential difference between the two visits in a univariate way [26]. The two visits may be between Visit 1 & 2, Visit 2 & 3, and Visit 1 & 3. A significance level of less than or equal to 5% is considered statistically significant. Receiver Operating Characteristics (ROC) analysis is performed on significant radiomic features to assess the discriminatory power quantitatively by AUROC, $F1_{max}$, sensitivity, and specificity. MedCalc software is used for all the analyses in this study.

3 Results

The T1-weighted sagittal MR images considered in this study are from the openly available database from TCIA. Twenty-five patients of stage II/III before, after the first cycle, and end of the NACT treatment, are used for this study. The average age of the subjects is 46.12 ± 8.55 years with a range of 33 to 67 years.

The representative set of DCE-MR images of three visits for PCR subjects is shown in Figure 1 (a–h) followed by mean intensity curves. From Figure 1 (a–c) it is observed that the heterogeneously enhanced circumscribed shaped mass of smooth margins in the Visit 1 of 46 years old female patient is altered in the shape such as thinning the size of the tumor after the first cycle of NACT treatment (Visit 2) and then completely responding at the end of NACT (Visit 3). This might be owing to suppression of the tumor due to NACT and low perfusion of the tumor. Similarly, Figure 1 (e–g) represents a rim-enhanced tumor with an irregular shape that invades the surrounding tissues. The necrotic component inside the tumor region is observed to be reduced after NACT treatment as a result of increased apoptosis. Figure 1 (d, h) represents the corresponding mean intensity curves at all three visits of a patient.

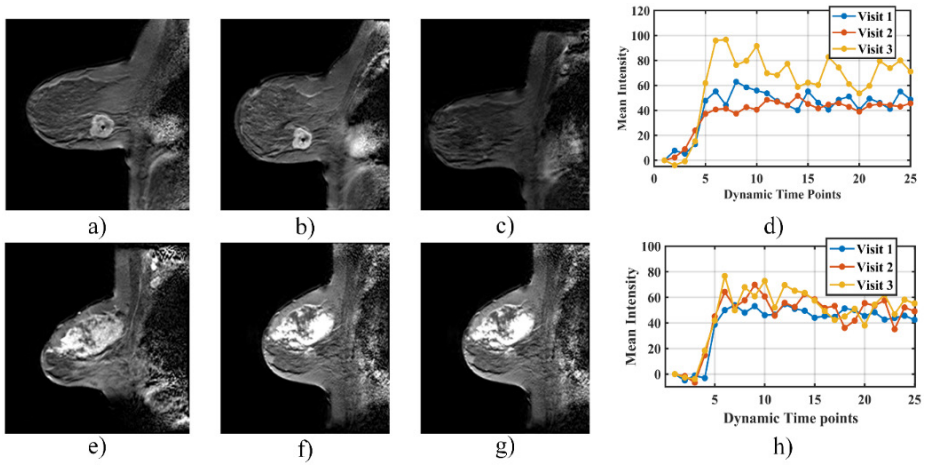

Fig. 1. (a–h) DCE-MR images of two PCR patients represented in each row at Visit 1 (column 1), Visit 2 (column 2), Visit 3 (column 3), and corresponding time points versus mean intensity curves (column 4)

In the same way, Figure 2 (a–h) represents a typical set of images of non-PCR subjects at three visits with mean intensity curves in the last column. From Figure 2 (a–c), a heterogeneous internal enhanced irregular shaped tumor with spiculated margins can be observed in all the visits. There is no distinguishable change in the tumor is observed during the NACT treatment. Likewise in Figure 2 (e–g), an aggressive tumor with dark internal septation present is reduced after the first cycle of the treatment through the end of NACT, but no acceptable change in the shape of the tumor can be observed. So, the response study of the NACT treatment poses challenges in identifying the usefulness of radiomics and alters the treatment planning.

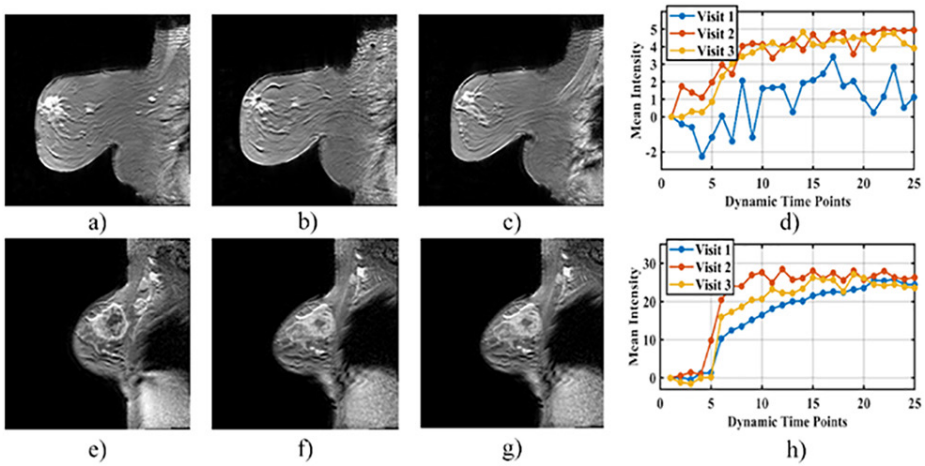

Fig. 2. (a-h) DCE-MR images of two non-PCR patients represented in each row at Visit 1 (column 1), Visit 2 (column 2), Visit 3 (column 3), and corresponding time points versus mean intensity curves (column 4)

Based on the mean intensity calculated at each time point of three visits, the time point with maximum mean intensity is used for applying the Gabor filter. The Gabor filter bank with $\lambda = 2$ and $\theta = (0°,30°,60°,90°,120°,135°,150°)$ are applied on the maximum mean intensity time point volume. The filtered image set for all the selected parameter combinations is shown in Figure 3. From the statistical Analysis 35 radiomic features stemming from three different comparisons between Visit 1 & 2, Visit 2 & 3, and Visit 1 & 3 were having a statistical difference with a p-value ≤ 0.05. Specifically, 14 features from $\lambda = 2$ and $\theta = 30°$ and 10 features from $\lambda = 2$ and $\theta = 120°$, and 11 features from $\lambda = 2$ and $\theta = 135°$ exhibit a significant difference. Each feature is calculated in three different visits, Visit 1, Visit 2, and Visit 3 separately.

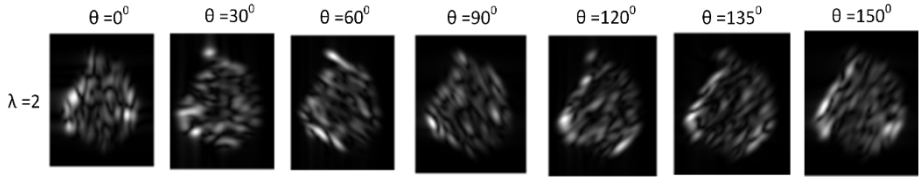

Fig. 3. Gabor filtered DCE-MR image illustrated for $\lambda = 2$ and $\theta = (0°,30°,60°,90°,120°,135°,150°)$

The significant Gabor derived radiomic features at $\lambda = 2$ and $\theta = 30°,135°,120°$ are presented in Table 2. The Variance between Visits 1 & 3 has shown a significance with $P \leq 0.05$ but there is no noticeable difference between Visit 1 to 2 and Visit 2 to 3. Low significance invariance represents the pixel intensities are closer to the mean of the image set. The subtle difference in the tumor region is observed to be less when compared to Visit 1 Vs 3. The GLCM features energy, entropy, SumAverage and autocorrelation have shown a significant difference between Visit 2 & 3 with p-values of 0.01134, 0.0061, 0.0418, and 0.0348 respectively. Similarly, these features have shown

a difference between Visits 1 & 3 except for the energy and entropy with p values 0.0252 and 0.0214. The change in tumor heterogeneity for treatment response analysis is also confirmed by GLRLM and GLSZM features, a prevailing technique for quantifying the texture homogeneity or heterogeneity.

Table 2. Comparative analysis of significant radiomic features at Gabor filter settings $\lambda = 2$ and $\theta = 30°,135°,120°$

Feature List	GF_λ = 2_θ = 30° (P-Value)			GF_λ = 2_θ = 135° (P-Value)			GF_λ = 2_θ = 120° (P-Value)		
	V1&V2	**V2&V3**	**V1&V3**	**V1&V2**	**V2&V3**	**V1&V3**	**V1&V2**	**V2&V3**	**V1&V3**
Variance	0.1204	0.4658	**0.0572**	0.4269	0.4723	0.4155	0.4225	**0.032**	**0.0261**
Skewness	0.4647	0.2546	0.1146	0.3765	0.2516	0.1964	0.1007	0.0667	**0.0019**
Kurtosis	0.3691	0.1895	0.1034	0.3819	0.2995	0.2286	**0.0588**	0.1477	**0.0056**
Energy	0.1578	**0.0113**	0.3045	0.2664	**0.0533**	**0.0319**	0.4844	**0.0155**	**0.0186**
Entropy	0.2179	**0.0061**	0.0689	0.4045	**0.0438**	**0.04**	0.1636	0.1636	0.1724
SumAverage	0.3165	**0.0418**	**0.0252**	0.4792	**0.0535**	0.0676	0.1631	0.1666	0.0642
Auto Correl	0.3317	**0.0348**	**0.0215**	0.4993	**0.0443**	0.0723	0.1595	0.4849	0.0665
SRE	0.3752	0.0884	**0.0432**	0.4841	**0.0316**	**0.0554**	0.2746	0.1723	0.1064
GLN	0.1636	**0.0256**	0.1636	0.1737	**0.0128**	0.1054	0.2235	**0.0576**	0.2118
LGRE	0.1876	0.2588	0.4193	0.3665	0.1318	0.2375	0.3803	0.0677	**0.0543**
SRLGE	0.1636	0.0863	0.1636	0.4145	**0.0512**	**0.0429**	0.0988	0.0763	**0.0042**
HGRE	0.2688	**0.0489**	0.3105	0.4932	0.0817	0.1343	0.4935	0.1264	0.1543
LRHGE	0.2479	**0.0336**	0.1846	0.4723	**0.0433**	0.0952	0.4925	0.0604	0.0972
SZE	0.3963	0.0885	**0.0489**	0.4841	0.1114	0.1256	0.2746	0.1723	0.1062
GLN	0.2298	**0.0256**	0.1052	0.1737	**0.0187**	0.1336	0.2235	**0.0576**	0.2118
LGZE	0.4942	0.1181	0.1706	0.3665	0.1039	0.1261	0.3803	0.0677	**0.0543**
HGZE	0.4822	**0.0489**	0.0664	0.4932	0.0861	0.1467	0.4935	0.1264	0.1543
SZLGE	0.3460	0.0863	**0.0483**	0.4145	**0.0579**	**0.0483**	0.0988	0.0763	**0.0042**
LZHGE	0.3674	**0.0336**	**0.0264**	0.4723	**0.0477**	0.1054	0.4925	0.0604	0.0972

Gray Level Non-uniformity in both GLRLM and GLSZM has reported a better significant difference with a p-value of 0.0256 among other significant features. Thus, by comparing all the radiomic features from the filtered image, entropy between Visit 2 & 3 have been observed to have a high quantifiable difference compared to the other two combinations with a p-value of 0.00605.

The features from the Gabor filter bank of $\lambda = 2$ and $\theta = 135°$ have shown a difference from Visit 2 to 3 and very few parameters from Visit1 to Visit 3. The Non-uniformity feature from Run length and size zone feature classes has been shown a significant difference with a p-value of 0.0128. Similarly, the Gabor filter with $\lambda = 2$ and $\theta = 120°$ have reported a highly significant difference between Visit 2 to Visit 3 and Visit 1 to 3. Most of the features have shown a difference from Visit 1 to 3 than Visit 2 to 3. Skewness and kurtosis features from Vist 1 to 3 have shown highly significant p-values of 0.001 and 0.005 respectively.

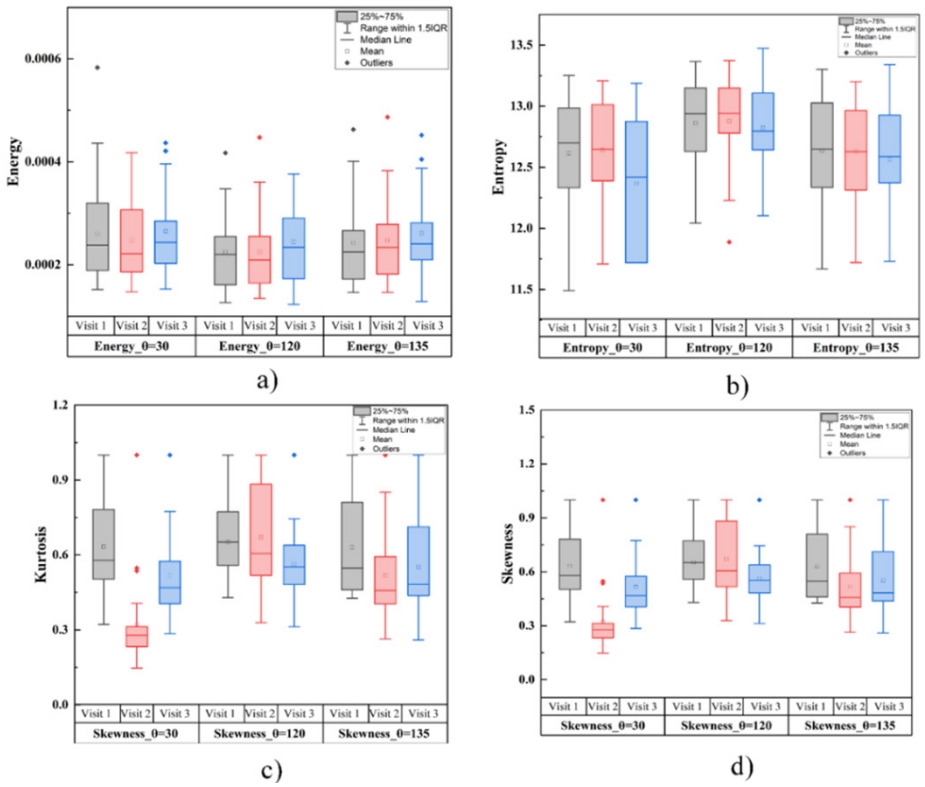

Fig. 4. Box-plot representation of radiomic features comparing three NAC treatment visits observed at θ = 30°, 120°, 135° of (a) Energy (b) Entropy (c) Kurtosis and (d) Skewness

The box-plot representation of a few Gabor derived radiomic features that could discriminate the pathological changes in NACT treatment visits at λ = 2 and θ = 30°, 120°, and 135° are shown in Figure 4 (a–d). It is observed from Figure 4 (a) that mean values of Energy remained similar in Visit 2 & 3 when compared to Visit 1 in both 30° and 120° orientations. But there is a change in Energy from Visit 1, Vist 2 to Visit 3 in θ = 135°. This illustrates that an Energy of Gabor filter at λ = 2 and θ = 135° settings can be used for NACT treatment response analysis between different visits. The radiomic features extracted from the 120° orientation are observed to have the most significant difference between the visits compared to the other two orientations (30° and 135°). Similarly, Entropy from Figure 4 (b) has shown a difference from Visit2 to Visit3 more compared to Visit1 to Visit 3. The response from Visits 1 to 2 did not provide an acceptable difference in all the orientations. Kurtosis and skewness in Figure 4 (c & d), show an adequate difference between Visit 1 & 3 in all the orientations with decreased heterogeneity and protruding better NACT response.

Table 3. ROC analysis of the most significant radiomic features

Feature Name	Feature Class	Significant Visits	AUROC	Sensitivity	Specificity	$F1_{max}$	Asymptotic Probability
GF_λ = 2 _30deg_SRE	GLRLM	V1&V3	76.38	68.2	82.1	71.4	0.0014
GF_λ = 2 _30deg_SZE	GLSZM	V1&V3	75.16	50	96.4	68.3	0.0024
GF_λ = 2 _135deg_Energy1	GLCM	V1&V3	71.10	77.3	60.7	68	0.011
GF_λ = 2 _135deg_Energy	GLCM	V2&V3	69.15	86.4	50	69.1	0.0211
GF_λ = 2 _135deg_SRE1	GLRLM	V1&V3	67.04	45.5	89.3	65.5	0.0401
GF_λ = 2 _135deg_GLN1	GLSZM	V2&V3	65.74	81.8	50	66.7	0.0579
GF_λ = 2 _30deg_GLN	GLRLM	V2&V3	65.26	77.3	57.1	66.7	0.0661
GF_λ = 2 _30deg_GLN1	GLSZM	V2&V3	65.26	77.3	57.1	66.7	0.0661

Table 3 demonstrates the ROC analysis of the most significant radiomic features that attain the highest AUROC to assess the discriminative power of the radiomic feature in treatment response. The sensitivity, specificity, $F1_{max}$, and asymptotic probabilities are listed accordingly. It is observed that SRE of $\lambda = 2$ and $\theta = 30°$ from Visit 1 uncovered a better predictive performance in Visit 3 with an AUROC value of 76.38%, the sensitivity of 68.2%, sensitivity of 82.1%, $F1_{max}$ of 71.4%, and probability of $P \leq 0.001$. Similarly, SZE from 30° and Energy from 120° between Visit 1 & 3 exhibited an AUROC values of 75.16% and 71.10%, sensitivity of 50% and 77.3%, specificity of 96.4% and 60.7%, $F1_{max}$ of 68.3% and 68% with p-values 0.002 and 0.01 respectively. The ROC curve for the three highest AUROC is plotted as shown in Figure 5.

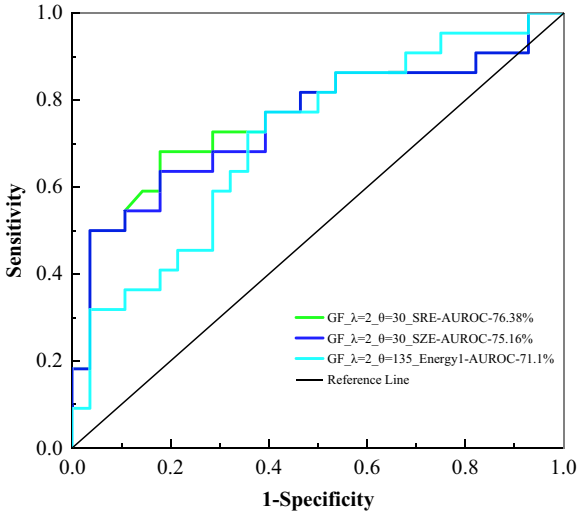

Fig. 5. ROC curve of radiomic features SRE at $\lambda = 2$ and $\theta = 30°$, SZE at $\lambda = 2$ and $\theta = 30°$ and Energy1 at $\lambda = 2$ and $\theta = 135°$

4 Discussion

In this current study, the Gabor derived radiomic features are extracted from DCE-MR images to assess the NACT treatment response between the visits. A total of 25 QIN-Breast dataset are considered for this study at three different time points prior to start of the treatment (Visit 1), after the first cycle of treatment (Visit 2), and at the end of the NACT treatment (Visit 3). Three different comparisons are examined between Visit 1 & 2, Visit 2 & 3, Visit 1 & 3. Thirty-eight radiomic features are extracted from all three visits of treatment using different Gabor filter parameter combinations of scale $\lambda = 2$ and $\theta = (0°,30°,60°,90°,120°,135°,150°)$. A radiomic analysis context from 4 different feature types Global, GLCM, GLRLM, and GLSZM were calculated for each visit of data.

The vascular changes in the tumor due to NACT treatment are observed to be sensitive. Subsequently, the prediction and classification of treatment response become consistently challenging because of the homogeneous nature of the tumors. Hence three Gabor parameter settings are used to compare the individual visits in terms of radiomic analysis. Reports of radiomic analysis have shown importance in determining therapy response during NACT. Several studies used this radiomic analysis in the classification and prediction of treatment response with different settings based on the nature of the dataset and the performance calculations [9,27–30].

Limited studies are reported and conducted for Gabor filter-based NACT treatment response using radiomics. The response of the treatment in those studies is carried out at two time points i.e., before and after the treatment. The performance of this study is carried out by comparing three different treatment visits using the same QIN BREAST dataset from TCIA.

Braman et al., [20] used radiomic feature analysis for intratumor and peritumoral regions of the breast tumors to predict the pre-treatment response to NACT. PCR prediction is performed among all corners and by separation of receptor type. The Gabor features median, skewness in initial phase, and kurtosis at the peak phase are reported as some of the prominent radiomic features in the prediction of pre-treatment response to NACT. However, it has been stated that the selection of molecular subtype subjects within Triple Negative (TN)/Human Epidermal Growth Receptor (HER2+) leads to loss of tumor information due to inter-observer variability and has the drawback of its performance in prediction of response. Another study produced by Manikis et al., [31] could predict breast cancer therapy response using Gabor filtered radiomic analysis. The performance of this study is implemented by extracting four different feature classes from multi-scale and orientation filtered images and validated with gradient boosting classifiers. This method of prediction is performed between the baseline and end of the NACT treatment, rather it could be studied with every treatment cycle for the patient's response.

The results indicate that the NACT treatment response can be assessed either in three comparisons of treatments Visit 1 (pre-treatment), Visit 2 (first cycle of NACT) and Visit 3 (end of NACT/prior to surgery). The Gabor settings of $\lambda = 2$ and $\theta = 30°$, 120°, 135° are used to compare the individual visits. Energy from all the orientations has shown a distinguishable change between Visits 2 & 3. The energy which measures the degree of randomness in the intensity values exhibited consistent tumor image intensities from Visit 2 to 3. The critical characteristic of the tumor is abnormal energy metabolism. The vascularity changes in the malignant tumors are observed to have a difference in energy due to their microvascular structure. The subtle difference in the tumor region is observed to be less when compared to Visit 1 Vs 3. Variance is more for the cancer cells as the contrast leakage will change abruptly with respect to time. This caused a noticeable change between the first cycle of the tumor area and at the end of the scans which can quantify the irregularity of the lesions. Entropy is related to the heterogeneity and complexity of lesion texture. The texture feature is presumably associated with a smooth margin, homogeneous, and lower enhancements of a benign lesion in comparison with an irregular margin, heterogeneous, and higher enhancements of a malignant lesion.

Gray Level Non-uniformity has shown a quantifiable difference in the visits as the gray level outliers at Visit2 & 3 differ from Visit 1 that results in a significant change between the visits. The group of voxels in the tumor that have the same gray level in the first cycle of NACT (Visit 2) changes slightly during Visit 3 due to a change in the flow rate of the contrast medium. This shows the tumor is rendered in the tumor region due to a decrease in affected tissue vascularity. Skewness and kurtosis from Vist 1 to 3 have shown a significant difference at $\lambda = 2$ and $\theta = 120°$. Asymmetry and flatness of intensities in the tumor region replicate the tumor spatial heterogeneity. The significant skewness and kurtosis indicate that the position and distribution patterns after the first cycle of NACT become more positive compared to the previous visits. This change in value is correlated to the characteristics of contrast enhanced tumors that include heterogeneity of angiogenesis, and microvasculature.

It is observed that the treatment response is significant from Visit 2 to Visit 3 and from Visit 1 to 3. The biological characteristics of the lesion from pre-treatment screening

to the first cycle of NACT are observed to have no change as the median time of 14 days with a range of 7 to 29 days is reported. Thus, no significant change between the visits is noticed in any scale-orientation Gabor analysis. The change in micro-vessel density, lesion angiogenesis, and structural disorders can be observed from the early treatment to the end of the NACT treatment. So, the change in tumor heterogeneity can be perceived quantifiably and show a statistical difference during the visits. Hence it is required to assess the treatment response at early stages to optimize treatment planning and help in decision making.

Further to extend the analysis and to investigate the diagnosing ability of statistically significant features at multiple orientations and one scale, ROC Analysis has been performed. It can be observed that the best radiomic features were SRE, SZE, and energy by achieving an AUROC of 76.38%, 75.16%, and 71.10% respectively. The fine texture has more short runs compared to the coarse texture. The contrast enhanced tumor region tends to have a fine texture portion after the DCE exam performed during NACT. This might be the reason to have a significant difference in Visits 2 & 3 with respect to Visit 1. The distribution of homogeneous regions is defined by SZE and found to be more after and at the end of the treatment. The malignant lesions characterized by angiogenesis were associated with aggressive nature compared to benign lesions. Moreover, energy increases with an increase in the uniformity of the pixels from Visit 1 to 3. $F1_{max}$ is measured to test the accuracy between the comparisons and asymptotic probability is a significant level where the probability of area under the curve is found correct.

Interestingly, preliminary results from [32,33] reported that the radiomic features alone can differentiate the treatment response before and after the treatment. While a couple of studies have been conducted in NACT treatment response, they have been used either first follow-up NACT data or/and the end of the NACT data. However, these findings were obtained using different data sources but have yet to be validated. Previous findings have not been limited to this condition, but eventually proposed a radiomics based breast malignancy index (RBMI) to find the pathological changes during NACT treatment [34]. The treatment response at every stage of NACT could help for early detection of the response. This quantitative study suggests that scale-orientation based Gabor filters are used as an instinctive method to explore the efficiency of radiomic features in multiple orientations and scales. This method provides a structured way to investigate the scale-orientation consistency of potential features, and these findings show that important radiomic features can be found in several best scale orientation statistical settings which demonstrates higher robustness.

There are a few limitations in the study. The patient cohort used in this analysis is very small and considered to be a preliminary result. It is observed that they show the potential of radiomic features to assess the NACT treatment response and compare the response of the treatment at Visit 1, Visit 2, and Visit 3 of NACT observed in multiple scales and orientations. In the future, machine learning methods are used to quantitatively predict the NACT treatment response.

5 Conclusion

The NACT treatment response for breast cancer patients has great importance clinically that can improve the prognosis and disease-free survival. In this study, an attempt is made to quantify the tumor changes with radiomic analysis on Gabor derived DCE-MR images. The data is collected from QIN Breast of TCIA which contains 68 subjects. A total of 25 patients' data is considered for three different time points Visit 1, Visit 2, and Visit 3. Radiomic features which include global, GLCM, GLRLM, and GLSZM features are extracted using MATLAB and statistically tested between the individual visits using MedCalc software. Specifically, results demonstrate that the radiomic signatures for treatment response from Visit 2 to Visit 3 at $\lambda = 2$ and $\theta = 30°$, at $\lambda = 2$ and $\theta = 135°$, and Visit 1 to Visit 3 at $\lambda = 2$ and $\theta = 120°$ remained significant. Further, the SRE and SZE features at $\lambda = 2$ and $\theta = 30°$ and energy at $\lambda = 2$ and $\theta = 135°$ are prominent radiomic features that exhibited the discriminant power with an AUROC of 76.38%, 75.16%, and 71.10% respectively. In conclusion, this study has been used for identifying the radiomic feature that could assess the response of the treatment in different scales and orientations, however, this method is not used to explore scale and orientation in radiomics analysis. Hence, findings from this study potentially hold radiomic features in different Gabor settings that could help clinicians for assessing the treatment response that allows the identification of patients who respond to the NACT treatment.

6 Acknowledgment

The authors thank Dr. K. R. Anandh for continuous support and proofreading of this manuscript.

7 References

[1] H. Sung, J. Ferlay, R.L. Siegel, M. Laversanne, I. Soerjomataram, A. Jemal, F. Bray. (2021). Global Cancer Statistics 2020: GLOBOCAN Estimates of Incidence and Mortality Worldwide for 36 Cancers in 185 Countries, CA. Cancer J. Clin. 71:209–249. https://doi.org/10.3322/caac.21660

[2] A.M. Thompson, S.L. Moulder-Thompson. (2012). Neoadjuvant Treatment of Breast Cancer, Ann. Oncol. 23. https://doi.org/10.1093/annonc/mds324

[3] S. Iranmakani, T. Mortezazadeh, F. Sajadian, M.F. Ghaziani, A. Ghafari, D. Khezerloo, A.E. Musa. (2020). A Review of Various Modalities in Breast Imaging: Technical Aspects and Clinical Outcomes, Egypt. J. Radiol. Nucl. Med. 51. https://doi.org/10.1186/s43055-020-00175-5

[4] C.K. Kuhl, R.K. Schmutzler, C.C. Leutner, A. Kempe, E. Wardelmann, A. Hocke, M. Maringa, U. Pfeifer, D. Krebs, H.H. Schild. (2000). Breast MR Imaging Screening in 192 Women Proved or Suspected to Be Carriers of a Breast Cancer Susceptibility Gene: Preliminary Results, Radiology. 215:267–279. https://doi.org/10.1148/radiology.215.1.r00ap01267

[5] M.L. Marinovich, F. Sardanelli, S. Ciatto, E. Mamounas, M. Brennan, P. Macaskill, L. Irwig, G. von Minckwitz, N. Houssami. (2012). Early Prediction of Pathologic Response to Neoadjuvant Therapy in Breast Cancer: Systematic Review of the Accuracy of MRI, Breast. 21:669–677. https://doi.org/10.1016/j.breast.2012.07.006

[6] V. Dialani, T. Chadashvili, P.J. Slanetz. (2015). Role of Imaging in Neoadjuvant Therapy for Breast Cancer, Ann. Surg. Oncol. 22:1416–1424. https://doi.org/10.1245/s10434-015-4403-9

[7] B.J. Song, S.H. Kim, A. Lee, Y. Kim, B.J. Kang, K. Yim, Y. Nam. (2018). Early Prediction of Response to Neoadjuvant Chemotherapy Using Dynamic Contrast-Enhanced MRI and Ultrasound in Breast Cancer, Korean J. Radiol. 19:682. https://doi.org/10.3348/kjr.2018.19.4.682

[8] A. Ashraf, B. Gaonkar, C. Mies, A. Demichele, M. Rosen, C. Davatzikos, D. Kontos. (2015). Breast DCE-MRI Kinetic Heterogeneity Tumor Markers: Preliminary Associations with Neoadjuvant Chemotherapy Response, Transl. Oncol. 8:154–162. https://doi.org/10.1016/j.tranon.2015.03.005

[9] G. Thibault, A. Tudorica, A. Afzal, S.Y. Chui, A. Naik, M.L. Troxell, K.A. Kemmer, K.Y. Oh, N. Roy, N. Jafarian, M.L. Holtorf, W. Huang, X. Song, G. Thibault. (2017). DCE-MRI Texture Features for Early Prediction of Breast Cancer Therapy Response, Tomography. 3:23–32. https://doi.org/10.18383/j.tom.2016.00241

[10] R. Varaprasada Rao, & T. Jaya Chandra Prasad. (2021). A New Optimized Hybrid Local Lifting Wavelet Co-Occurrence Texture Pattern for Content Based Medical Image Retrieval. International Journal of Online and Biomedical Engineering (iJOE), 17(11), pp. 157–175. https://doi.org/10.3991/ijoe.v17i11.25351

[11] H. M. Amer, F. E. Abou-Chadi, S. S., Kishk, & M. I. Obayya. (2019). A CAD System for the Early Detection of Lung Nodules Using Computed Tomography Scan Images. International Journal of Online and Biomedical Engineering (iJOE), 15(04), pp. 40–52. https://doi.org/10.3991/ijoe.v15i04.9837

[12] H.J.W.L.A. Stephen SF Yip. (2017). Applications and Limitations of Radiomics Stephen, Phys Med Biol. 176:139–148. https://doi.org/10.1088/0031-9155/61/13/R150.Applications

[13] E. Scalco, G. Rizzo. (2017). Texture Analysis of Medical Images for Radiotherapy Applications, Br. J. Radiol. 90. https://doi.org/10.1259/bjr.20160642

[14] J.G. Daugman. (1988). Complete Discrete 2-D Gabor Transforms by Neural Networks for Image Analysis and Compression, IEEE Trans. Acoust. 36:1169–1179. https://doi.org/10.1109/29.1644

[15] A. Bodnarova, M. Bennamoun, S. Latham. (2002). Optimal Gabor Filters for Textile Flaw Detection, Pattern Recognit. 35:2973–2991. https://doi.org/10.1016/S0031-3203(02)00017-1

[16] K.R. Namuduri, R. Mehrotra, N. Ranganathan. (1992). Edge Detection Models based on Gabor Filters, Proc.—Int. Conf. Pattern Recognit. 3:729–732. https://doi.org/10.1109/ICPR.1992.202090

[17] J. Yang, L. Liu, T. Jiang, Y. Fan. (2003). A Modified Gabor Filter Design Method for Fingerprint Image Enhancement, Pattern Recognit. Lett. 24:1805–1817. https://doi.org/10.1016/S0167-8655(03)00005-9

[18] F. Mirzapour, H. Ghassemian. (2013). Using GLCM and Gabor Filters for Classification of PAN Images, In: 2013 21st Iran. Conf. Electr. Eng., pp. 1–6. https://doi.org/10.1109/IranianCEE.2013.6599565

[19] L. Chen, G. Lu, D. Zhang, Effects of Different Gabor Filters Parameters on Image Retrieval by Texture, In: 10th Int. Multimed. Model. Conf. 2004. Proceedings., 2004: pp. 273–278. https://doi.org/10.1109/MULMM.2004.1264996

[20] N.M. Braman, M. Etesami, P. Prasanna, C. Dubchuk, H. Gilmore, P. Tiwari, D. Pletcha, A. Madabhushi. (2017). Intratumoral and Peritumoral Radiomics for the Pretreatment Prediction of Pathological Complete Response to Neoadjuvant Chemotherapy Based on Breast DCE-MRI, Breast Cancer Res. 19:1–14. https://doi.org/10.1186/s13058-017-0846-1

[21] Z. Liu, Z. Li, J. Qu, R. Zhang, X. Zhou, L. Li, K. Sun, Z. Tang, H. Jiang, H. Li, Q. Xiong, Y. Ding, X. Zhao, K. Wang, Z. Liu, J. Tian. (2019). Radiomics of Multiparametric MRI for Pretreatment Prediction of Pathologic Complete Response to Neoadjuvant Chemotherapy in Breast Cancer: A Multicenter Study, Clin. Cancer Res. 25:3538–3547. https://doi.org/10.1158/1078-0432.CCR-18-3190

[22] K. Clark, B. Vendt, K. Smith, J. Freymann, J. Kirby, P. Koppel, S. Moore, S. Phillips, D. Maffitt, M. Pringle, L. Tarbox, F. Prior. (2013). The Cancer Imaging Archive (TCIA): Maintaining and Operating a Public Information Repository, J. Digit. Imaging. 26:1045–57. https://doi.org/10.1007/s10278-013-9622-7

[23] X. Li, R.G. Abramson, L.R. Arlinghaus, H. Kang, A.B. Chakravarthy, V.G. Abramson, J. Farley, I.A. Mayer, M.C. Kelley, I.M. Meszoely, J. Means-Powell, A.M. Grau, M. Sanders, T.E. Yankeelov. (2015). Combined DCE-MRI and DW-MRI for Predicting Breast Cancer Pathological Response After the First Cycle of Neoadjuvant Chemotherapy, Invest. Radiol. 50:195–204. https://doi.org/10.1097/RLI.0000000000000100

[24] A.K. Jain, F. Farrokhnia. (1991). Unsupervised Texture Segmentation using Gabor Filters, Pattern Recognit. 24:1167–1186. https://doi.org/10.1016/0031-3203(91)90143-S

[25] B. Dhruv, N. Mittal, M. Modi. (2019). Study of Haralick's and GLCM Texture Analysis on 3D Medical Images, Int. J. Neurosci. 129:350–362. https://doi.org/10.1080/00207454.2018.1536052

[26] P. Mishra, U. Singh, C.M. Pandey. (2019). Application of Student's t-test, Analysis of Variance, and Covariance, 407–411. https://doi.org/10.4103/aca.ACA_94_19

[27] A. Tudorica, K.Y. Oh, S.Y.C. Chui, N. Roy, M.L. Troxell, A. Naik, K.A. Kemmer, Y. Chen, M.L. Holtorf, A. Afzal, C.S. Springer, X. Li, W. Huang. (2016). Early Prediction and Evaluation of Breast Cancer Response to Neoadjuvant Chemotherapy using Quantitative DCE-MRI, Transl. Oncol. 9:8–17. https://doi.org/10.1016/j.tranon.2015.11.016

[28] Zahedi, F., & Karimi Moridani, M. (2022). Classification of Breast Cancer Tumors Using Mammography Images Processing Based on Machine Learning: Breast Cancer Tumors Using Mammography Images. International Journal of Online and Biomedical Engineering (iJOE), 18(05), pp. 31–42. https://doi.org/10.3991/ijoe.v18i05.29197

[29] K. Drukker, A. Edwards, C. Doyle, J. Papaioannou, K. Kulkarni, M.L. Giger. (2019). Breast MRI Radiomics for the Pretreatment Prediction of Response to Neoadjuvant Chemotherapy in Node-Positive Breast Cancer Patients, J. Med. Imaging (Bellingham, Wash.). 6;34502. https://doi.org/10.1117/1.JMI.6.3.034502

[30] V. Romeo, G. Accardo, T. Perillo, L. Basso, N. Garbino, E. Nicolai, S. Maurea, M. Salvatore. (2021). Assessment and Prediction of Response to Neoadjuvant Chemotherapy in Breast Cancer: A Comparison of Imaging Modalities and Future Perspectives, Cancers (Basel). 13: 1–18. https://doi.org/10.3390/cancers13143521

[31] G.C. Manikis, M. Venianaki, I. Skepasianos, G.Z. Papadakis, T.G. Maris, S. Agelaki, A. Karantanas, K. Marias. (2019). Scale-Space DCE-MRI Radiomics Analysis based on Gabor Filters for Predicting Breast Cancer Therapy Response, Proc.—2019 IEEE 19th Int. Conf. Bioinforma. Bioeng. BIBE 2019. 994–1001. https://doi.org/10.1109/BIBE.2019.00185

[32] P.D. Moyya, M. Asaithambi, A.K. Ramaniharan. (2019). Extraction of Radiomic Features from Breast DCE-MRI Responds to Pathological Changes in Patients during Neoadjuvant Chemotherapy Treatment, IST 2019—IEEE Int. Conf. Imaging Syst. Tech. Proc. 1–5. https://doi.org/10.1109/IST48021.2019.9010068

[33] P.D. Moyya, M. Asaithambi, A.K. Ramaniharan. (2021). Radiomics Based Analysis of Breast Tumors in DCE-MRI Due to Neoadjuvant Treatment Therapy, In: V.L.N. Komanapalli, N. Sivakumaran, S. Hampannavar (Eds.), Adv. Autom. Signal Process. Instrumentation, Control, Springer Singapore, Singapore, pp. 2197–2204. https://doi.org/10.1007/978-981-15-8221-9_204

[34] P.D. Moyya, M. Asaithambi, A.K. Ramaniharan. (2021). Radiomics Based Breast Malignancy Index to Differentiate Pathological Changes Due To Neoadjuvant Chemotherapy, Biomed. Sci. Instrum. 57:219–227. https://doi.org/10.34107/YHPN9422.04219

8 Authors

Priscilla Dinkar Moyya received an M.Tech degree in Digital Electronics and Communication Engineering in 2013 from JNTU Kakinada. Now she is a research scholar in the School of Electronics Engineering, Vellore Institute of Technology, Vellore, Tamil Nadu, India. Her research interests include biomedical image processing particularly in developing methods in Neoadjuvant chemotherapy treatment response analysis.

Mythili Asaithambi is an Associate Professor in the Department of Sensor and biomedical Technology, School of Electronics Engineering (SENSE), at Vellore Institute of Technology, Vellore. She was awarded PhD at Madras Institute of Technology, Anna University. She received M.S (By research) from Madras Institute of Technology, Anna University. She received her bachelor degree in Electronics and Instrumentation Engineering from the Government College of Technology, Coimbatore, India. Biomedical signal and image processing, biomedical Instrumentation, artificial intelligence, respiratory mechanics, breast cancer studies, computational analysis on drug design, sensor networks.

Article submitted 2022-05-16. Resubmitted 2022-06-13. Final acceptance 2022-06-17. Final version published as submitted by the authors.